Earth and Planetary Science Letters 616 (2023) 118230

Contents lists available at ScienceDirect

Earth and Planetary Science Letters

journal homepage: www.elsevier.com/locate/epsl

Detecting strain with a fiber optic cable on the seafloor offshore Mount Etna, Southern Italy

Marc-André Gutscher [a,*], Lionel Quetel [b], Shane Murphy [a], Giorgio Riccobene [c], Jean-Yves Royer [a], Giovanni Barreca [d], Salvatore Aurnia [a,c], Frauke Klingelhoefer [a], Giuseppe Cappelli [a,b], Morelia Urlaub [e], Sebastian Krastel [f], Felix Gross [f], Heidrun Kopp [e,f]

[a] Geo-Ocean, Univ Brest, CNRS, Ifremer, Plouzané, France
[b] IDIL Fiber Optics, Lannion, France
[c] INFN-LNS, Catania, Italy
[d] Department of Biological, Geology and Environmental Science, University of Catania, Catania, Italy
[e] GEOMAR Helmholtz Centre for Ocean Research, Kiel, Germany
[f] Institute of Geosciences, Kiel University, Kiel, Germany

ARTICLE INFO

Article history:
Received 1 November 2022
Received in revised form 30 April 2023
Accepted 17 May 2023
Available online 31 May 2023
Editor: J.-P. Avouac

Keywords:
monitoring active faults
submarine fiber optic cables
laser reflectometry
strike-slip fault
strain cable
seabottom currents

ABSTRACT

Oceans cover more than 70 percent of the Earth's surface making it difficult and costly to deploy modern seismological instruments here. The rapidly expanding global network of submarine telecom cables offers tremendous possibilities for seismological monitoring using laser light. Recent pioneer studies have demonstrated earthquake detection using lasers in onland and submarine fiber optic cables. However, permanent strain at the seafloor has never before been measured directly as it happens. With this aim, we deployed a dedicated 6-km-long fiber optic strain cable, offshore Catania Sicily, in 2000 m water depth, and connected it to a 29-km long electro-optical cable for science use. We report here that deformation of the cable equivalent to a total elongation of 2.5 cm was observed over a 21-month period (from Oct. 2020 to Jul. 2022). Brillouin laser reflectometry observations over the first 10 months indicate significant strain (+25 to +40 microstrain) at two locations where the cable crosses an active strike-slip fault on the seafloor, with most of the change occurring between 19 and 21 Nov. 2020. The cause of the strain could be fault slip or seabottom currents. During the following 11 months, the strain amplitude increased to +45 to +55 microstrain, affecting a longer portion of the cable up to 500 m to either side of the first fault crossing. A sandbag experiment performed on the distal portion of the cable (3.2–6.0 km) starting Sept. 2021 demonstrates how the fiber optic cable deforms in response to an applied load and how the deformation signal partially dissipates over time due to the elastic properties of the cable. These preliminary results are highly encouraging for the use of BOTDR (Brillouin Optical Time Domain Reflectometry) laser reflectometry as a technique to detect strain at the seafloor in near real time and to monitor the structural health of submarine cables.

1. Introduction, state of the art and objectives

1.1. Fiber optic cables and monitoring technology

Studying earthquakes and crustal deformation is difficult and costly for the 70% of the Earth which is covered by the oceans. The use of submarine fiber optic cables as seismological monitoring tools is a promising new field to gain access to vast portions of the seafloor. A typical tool is laser reflectometry, which is performed by firing a laser pulse from one end into an optical fiber and as the laser light scatters off microscopic inhomogeneities in the fiber it produces several characteristic diffraction peaks (Rayleigh, Brillouin, Raman) (Muanenda et al., 2019) (Suppl. Fig. 1). Laser reflectometry using fiber optic cables measures fluctuations in temperature and strain and is often referred to as distributed sensing (Muanenda et al., 2019). The DAS (distributed acoustic sensing) technique, using Rayleigh laser reflectometry, has been demonstrated for earthquake detection and recording with on-land fiber optic cables (Lindsey et al., 2017; Jousset et al., 2018; Wang et al., 2018; Yu et al., 2019). DAS studies using submarine cables offshore California (Lindsey et al., 2019), Southern France (Sladen et

* Corresponding author.
E-mail address: gutscher@univ-brest.fr (M.-A. Gutscher).

https://doi.org/10.1016/j.epsl.2023.118230

al., 2019) and Belgium (Williams et al., 2019) recorded local and distant earthquakes and ocean waves and allowed identification of submarine fault zones. Similarly, ultra-precise metrology using time-delays on both onshore and offshore fiber optic cables, successfully observed earthquakes (Marra et al., 2018). More recently this technique was applied to identify the specific segment of a submarine telecom cable between two given repeaters, which detected an earthquake induced disturbance (Marra et al., 2022).

Laser reflectometry in fiber optic cables can potentially detect movement across active submarine faults in near real time. The BOTDR (Brillouin Optical Time Domain Reflectometry) technique is commonly used for structural health monitoring of major engineering structures (e.g. – dams, bridges, pipelines, etc.) and under ideal conditions can measure very small strains typically 10–500 microstrain) at very large distances (10–200 km) and at a spatial resolution of a few meters (Maraval et al., 2017). These detection limits are two orders of magnitude better than typical land-based geodetic techniques (like GNSS). Some BOTDR land studies involved monitoring geo-hazards, for instance slow creep of a landslide (Sun et al., 2016) or collapse of roadways over karst (sink-holes in limestone) (Jiang et al., 2016). One offshore BOTDR study monitored a submarine power cable (Zhao et al., 2014). A short (200 m long) fiber optic strain cable featuring a Michelson interferometer was deployed in 1900 m depth near the toe of the Cascadia accretionary wedge (90 km offshore Oregon) and successfully recorded earth tides (Zumberge et al., 2018). However, laser reflectometry has never before been used to detect fault movements and permanent deformation on the seafloor. The goal of this work, within the framework of the FOCUS project (https://www.geo-ocean.fr/Recherche/Projets-de-Recherche/ERC-FOCUS), is to test the use of laser reflectometry, and more specifically the BOTDR method to detect long-term strain at the seafloor. For this purpose a dedicated fiber optic strain cable was deployed offshore Sicily crossing a tectonic fault in order to monitor long-term deformation, examine and quantify the response of the optical fibers in the cable, including both loosely and tightly bound fibers.

1.2. Study area and previous geodetic studies

Our primary study area is the northernmost portion of the Alfeo Fault offshore Eastern Sicily, near Mount Etna volcano (Fig. 1) (Gutscher et al., 2019). This region has been struck by numerous devastating historical earthquakes (1693, 1783, 1905, 1908), whose source faults remain uncertain in many cases to this day (Goes et al., 2004). The tectonics of the East Sicily - Calabria region are controlled in large part by the NW directed subduction of a narrow domain of oceanic lithosphere of the Ionian Sea (Dellong et al., 2018), beneath Calabria and the NE tip of Sicily (see inset Fig. 1) causing slab roll-back and extension in the SE Tyrrhenian Sea back-arc domain (Cernobori et al., 1996; Gvirtzman and Nur, 1999; Faccenna et al., 2004; Polonia et al., 2011). While it is generally accepted that this narrow subduction zone is bounded by a lateral slab tear fault offshore Eastern Sicily (Faccenna et al., 2004; Govers and Wortel, 2005), there is ongoing debate on the exact location of this lithospheric scale fault, and which of the strike-slip and/or normal faults observed offshore are associated with this slab tear (Argnani and Bonazzi, 2005; Polonia et al., 2011; Gutscher et al., 2016 and references therein). Offshore East Sicily, a network of strike-slip faults has been mapped on the seafloor, both by multi-beam swath-bathymetry and by reflection seismic profiles (Gutscher et al., 2016; Maesano et al., 2020). The predominantly strike-slip Alfeo Fault system, extending nearly continuously over 150 km, from Mount Etna to the south-east, is one of the leading candidates for the surface expression of a deeply rooted lateral slab tear fault (Gutscher et al., 2016). Observation of significant tectonic movement along the Alfeo Fault system could help resolve this debate.

Onshore GNSS and satellite (Synthetic Aperture Radar) studies reveal a system of strike-slip and normal faults accommodating a gradual eastward gravitational collapse of the southeast flank of Mount Etna (Bonforte et al., 2011) (Fig. 1). From 2016 to 2018 an array of five seafloor geodetic instruments was deployed along the offshore prolongation of these faults and recorded a dextral strike-slip movement of 4 cm, occurring as a 1-week long slow slip event in May 2017 (Urlaub et al., 2018) (Fig. 1). This established the presence of an active submarine fault about 20 km to the east of Catania, an urban area of 1 million people. This submarine fault is crossed by a scientific submarine electro-optical cable deployed from the port of Catania to a constellation of seafloor observatories, 25 km east of Catania in 2100 m water depth, allowing connection of deep-sea experiments (Gutscher et al., 2019) (Fig. 1). To the southeast, the submerged Etna flank faults, merge with the Alfeo Fault system achieving a total length of 150 km, a structure first mapped in the past 10 years and whose seismic hazard remains unknown (Gutscher et al., 2017) (Fig. 1, inset).

2. Experimental set-up

A 29 km-long Main Electro Optical Cable (the MEOC, Fig. 1) is operated by the Laboratori Nazionali del Sud of the Italian National Institute for nuclear Physics (INFN-LNS) to host prototypes for the KM3NeT cosmic neutrino detector (www.km3net.org) since year 2005. The MEOC is part of the EMSO (European - Mediterranean multidisciplinary Seafloor Observatory) network (Favali et al., 2013). At a distance of about 20 km from the coast the MEOC bifurcates into two branches, ending with two electro-optical cable terminations known as Test Site North and Test Site South, both at approximately 2100 m water depth.

In October 2020, using the ROV (Remotely Operated Vehicle) Victor6000, a 6-km long submarine fiber optic cable (manufactured by Nexans), hereafter the FOCUS fiber optic cable, was deployed. The dedicated strain cable, the work and instruments described here are all part of the European funded FOCUS project (Fiber Optic Cable Use for Seafloor studies of earthquake hazard and deformation) (Gutscher et al., 2019). First, the cable was connected to Test Site South (TSS) via a junction box, hereafter named Y-JB (for "Y-junction box") (Fig. 2 top). The Y-JB, placed about 20 m away from TSS, is a subsea frame equipped with oil-filled electro-optical cable and ROV mateable electro-optical connectors, specially designed by FOCUS to split fibers and conductors from a single connector to allow joint operation of the FOCUS experiment and of the SMO/ONDE acoustic observatory (Riccobene, 2009) already deployed at TSS. Through the Y-JB connection, two fibers of the MEOC were dedicated to connect the additional 6-km-long FOCUS cable to shore. Then, using a specially designed deep-sea plow cable deployment system (Fig. 2, lower right), the FOCUS cable was laid down and buried 20 cm beneath the seafloor (where the terrain and seafloor conditions allowed) (Suppl. Fig. 2). The plow has a spring release tension drum, which is set to operate at a tension of 250 N (about 25 kg), but due to heterogeneous seafloor sediment properties and difficulties during deployment, a constant tension of the cable was seldom achieved. The cable was deployed along a zig-zag path crossing the mapped North Alfeo fault at four locations (Fig. 2, left). The 9-mm diameter cable contains 3 tightly bound fibers in the core, and 2 loose fibers in a small steel tube in the armoring layer (Fig. 2, upper right). Given that we had access to 2 live fibers from shore, and in order to create redundancy in the observations, we designed 2 optical paths, a two-fold loop and a three-fold loop. For the three-fold loop we are reporting here, the pathway first follows a loose fiber from the Y-junction box (about 20 m from TSS) to the end, where the deep-sea plow is

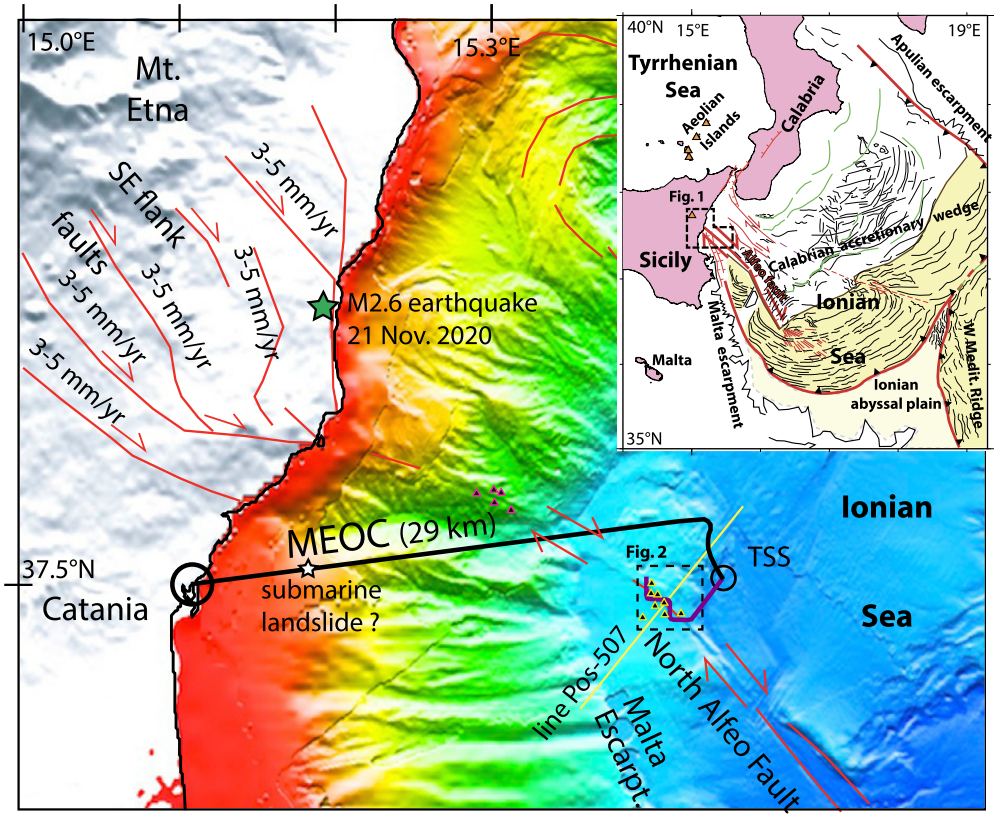

Fig. 1. Map of the Mount Etna - Catania region (Eastern Sicily) and nearby offshore (land in gray and bathymetry in color), showing the faults on the SE flank of Mount Etna and the offshore North Alfeo fault (red lines), the MEOC (Main Electro Optical Cable) operated by INFN-LNS[a] (thick black line), the seafloor observatory TSS[b] and the path of the 6-km long dedicated strain cable (shown in purple). Location of a seismic line imaging the sub seafloor sediments is shown (yellow line) (Gutscher et al., 2019). A small earthquake (magnitude 2.6) occurred on 21 Nov. 2020 at 13:55 (UTC) in Santa Venerina village (green star). The small white star indicates the position 6 km from the port of Catania where the cable was disturbed (possibly by a submarine landslide). Small magenta triangles are a network of 5 German seafloor geodetic stations deployed from May 2016 to Aug. 2018 (Urlaub et al., 2018). Small yellow triangles are a network of 8 French seafloor geodetic stations which operated from Oct. 2020 to Nov. 2021 (Royer et al., 2022). The dashed box indicates the location of Fig. 2. Inset: Simplified regional tectonic map (Gutscher et al., 2016, 2017) showing land in light gray - magenta (location of main part of Fig. 1 shown as dashed polygon) and yellow triangles are active volcanoes (Aeolian Islands and Mount Etna). [a] - *INFN-LNS is the physics institute of Catania: Istituto Nazionale di Fisica Nucleare - Laboratori Nazionali del Sud,* [b] - *TSS means Test Site South, a cabled seafloor observatory in 2060 m water depth, the Y-JB (Y-junction box shown in Fig. 2) is directly adjacent to TSS (20 m away, connected by an umbilical cable).*

located, then returns to Y-JB via a tightly bound fiber, and finally goes back out to the plow along a second tight fiber (Fig. 2, right inset). This optical path has a total length of 48 km. The strain along the fiber optic cable is measured using a VIAVI BOTDR interrogator (model T-BERD®/MTS-8000 DTSS), with an acquisition of several hundred thousand laser pulses over a nearly 2-hour period, and the backscatter from all these individual pulses detected by the interrogator is summed up and averaged in order to reduce the noise. The spatial sampling is one value every 2 meters along the cable.

3. Data/results

3.1. Laser reflectometry strain measurements Oct. 2020–Aug. 2021

The initial state of the cable was measured on 28 Oct. 2020 to establish a baseline from which the following results are presented. For the acquisition parameters used, the resolution of the BOTDR interrogator is typically <5 microstrain over the first 30 km, and then approaches 10 microstrain at distances of 40–50 km. Thus, if no strain has occurred, the difference with respect to the initial baseline should be <5–10 microstrain (the repeatability of a measurement at distances of 30–50 km). Indeed, this is the pattern observed in the 8 Nov. 2020 measurement (Fig. 3, top). In the measurement from 28 Aug. 2021, we observe distinct peaks at the first and third fault crossings, respectively, 2500 m and 4300 m from the Y-JB (Fig. 3, bottom, see also Suppl. Fig. 3). These peaks exhibit values ranging from +40 to +25 microstrain (in the tightly bound fibers) and about half that in the loosely bound fiber. The values are positive, which means the cable was elongated at these locations, a movement consistent with the dextral strike-slip motion predicted for this fault and observed 15 km further to the NW in May 2017 by the 2016–2018 deployment of seafloor geodetic stations (Urlaub et al., 2018) (Fig. 1). The peaks are expressed over lateral distances of several hundred meters (about 100–200 m for the smaller peak at the third fault crossing, and up to 400–500 m for the stronger peak at the first fault crossing). Integrating the curve above the 0 microstrain level allows us to quantify the estimated elongation and we obtain 1.0–1.5 cm for the first fault crossing and about 0.5 cm at the third fault crossing. All signals below the 0 micro-strain level represent cable shortening.

Most of the amplitude and spatial width of the elongation signals at the first and third fault crossings developed over a 2-day period, from 19–21 Nov. 2020 (Fig. 4). On 19 Nov. 2020, the vast majority of the BOTDR data are within ±10 microstrain from the 0 level. On 20 Nov. 2020, peaks begin to develop on all three fibers of the FOCUS fiber optic strain cable (the loose and the two tightly bound fibers) at a distance of 2.5 km from the Y-JB (see red arrows on Fig. 4). On 21 Nov. 2020, these peaks are well established and reach values of +15 to +20, +20 and +30 to +35 microstrain in the loose, tight1 and tight2 fibers, respectively (see also Suppl. Fig. 4). It is also worth noting along the MEOC, 6 km offshore Catania, there is a deformation event visible in the 20 and

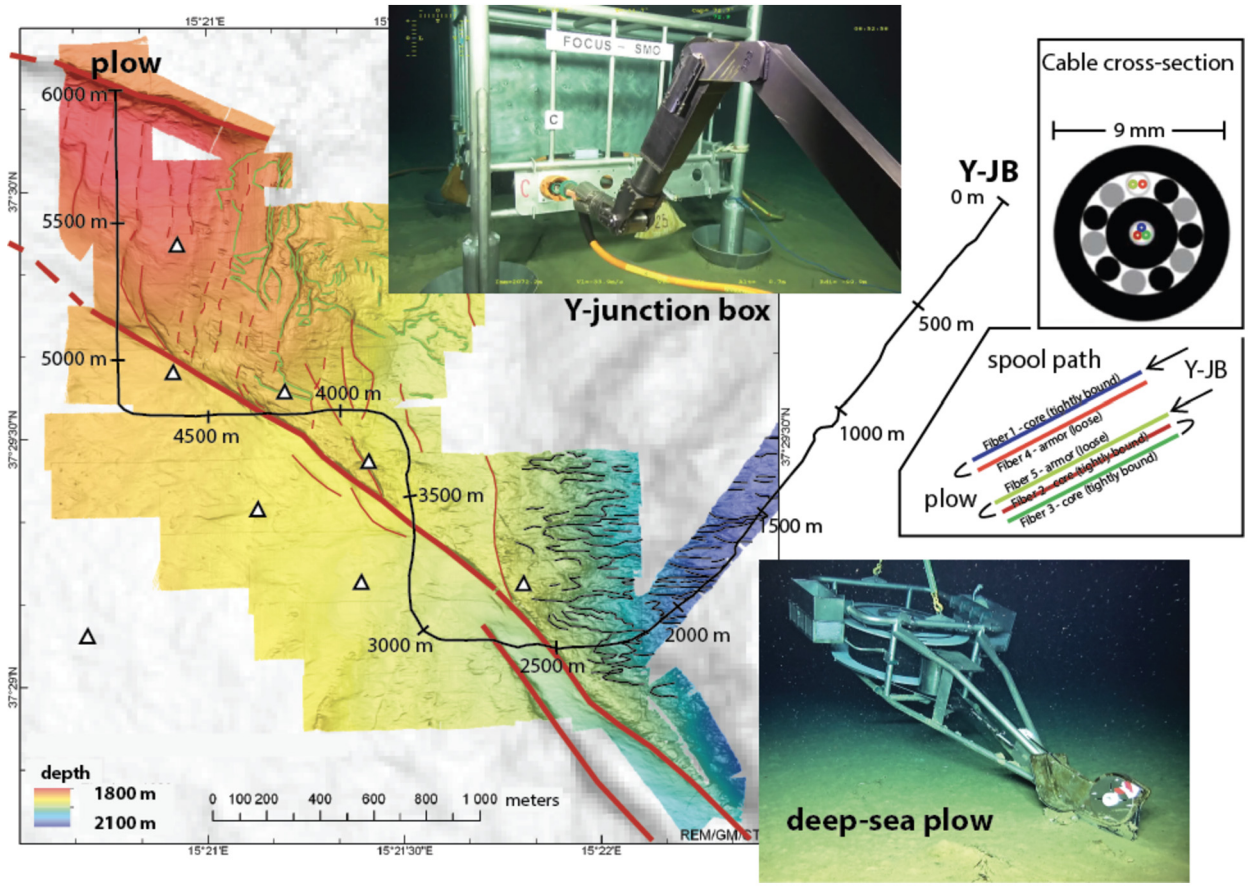

Fig. 2. (left) Track of the 6-km long fiber optic cable (black line) with distance along the track line in meters measured from the cabled observatory connection, the Y-junction box (Y-JB). Micro-bathymetric map (acquired by the ROV Victor6000 during the FocusX1 expedition) with interpretation: major fault trace (thick red line) and minor fault splays (thin red lines), submarine landslide (thin green lines) and an east-west trending system of gullies (thin black lines). Note the positions of the 1st fault crossing (at 2500 m cable track distance), 2nd fault crossing (at 3350 m cable track distance), 3rd fault crossing (at 4300 m cable track distance) and the 4th fault crossing (at 5150 m cable track distance). The positions of 8 seafloor geodetic stations are shown (white triangles) (Royer et al., 2022). 0 m is the position of the Y-JB (upper inset photo) and 6000 m the position of the deep-sea plow (lower inset photo), at the end of the optical path. (upper right) The cross-section of the 9 mm diameter fiber optic cable., (right inset) The two optical paths: a two-fold loop (12.4 km length) and a three-fold loop (18.6 km length) whose results are reported here.

21 Nov. 2020 records, with a dual signal of −15 microstrain (axial shortening) and +20 to +40 microstrain (elongation) (Fig. 4 middle and bottom). This signal develops over the same two-day period as the elongation event in the FOCUS strain cable (red arrows in Fig. 4, see also Suppl. Fig. 5).

The BOTDR observations in general are reliable and the elongation peaks described are robust features observed repeatedly at different time scales. For instance, 3 separate observations from 28 June, 28 July and 28 Aug. 2021 are shown and superposed for comparison (Fig. 5). The 100 m sliding averages are identical to within 5 microstrain and often even within 1–2 microstrain. The strong elongation peak at the first fault crossing and the more modest elongation peak observed at the third fault crossing are always present (Fig. 5). The same is true for the successive measurements conducted at intervals of 2 hours (Suppl. Fig. 6).

3.2. BOTDR observations since Sept. 2021 and results of the sandbag experiment

On 2–3 Sept. 2021 seafloor operations were performed with an ROV from an industry vessel (the Tidewater vessel Handin Tide, equipped and operated by Fugro) placing weight bags on 5 sections of the FOCUS fiber optic strain cable, located on the distal half, between 3.2 km and 6 km cable distance from the Y-JB (Fig. 6). These 5 sections of cable are each about 120 m in length. The main purpose was to try to improve the coupling between the FOCUS strain cable and the predominantly unconsolidated sediments at the seafloor. During cable burial operations performed in Oct. 2020, large portions of the cable could not be successfully buried due to rugged relief and/or the presence of indurated, highly viscous sediments. Therefore, over >50% of its length, the cable is lying on the seafloor or spanning across rugged relief (Suppl. Fig. 3). In Sept. 2021 a total of 79 sand-bags weighing 25 kg were placed in segments SB1 (23 bags); SB2 (24 bags); SB3 (21 bags) and SB4 (11 bags). 17 pellet bags (containing 4-mm sized steel pellets, weighing 25 kg each) were placed on the cable at 5.9 km cable distance, near the plow, which was also displaced 120 m to the north (using the Fugro ROV). The displacement was possible because there were 120 m of undeployed cable remaining on the plow-reel. Once the 120 m of cable had been paid out, the plow came to an abrupt halt, causing extreme strain in the cable, locally reaching values of +1000 micro-strain and −1000 microstrain (see Fig. 7B and Fig. 8). The locations of all 96 bag drops were recorded using the ultra short baseline acoustic positioning system installed onboard the ship and ROV. The error of the used system at such depth is about ±10 m (x, y, depth). A photo of the sand-bag drop operations is shown (Fig. 6B).

BOTDR data for the proximal 3 km over the period Sept. 2021–late July 2022 indicate additional strain accumulation at the first fault crossing (Fig. 7, Fig. 8). During this period, a larger, broader deformation signal developed across a nearly 1-km long section of cable (from 2.0–3.0 km cable distance from the Y-JB),

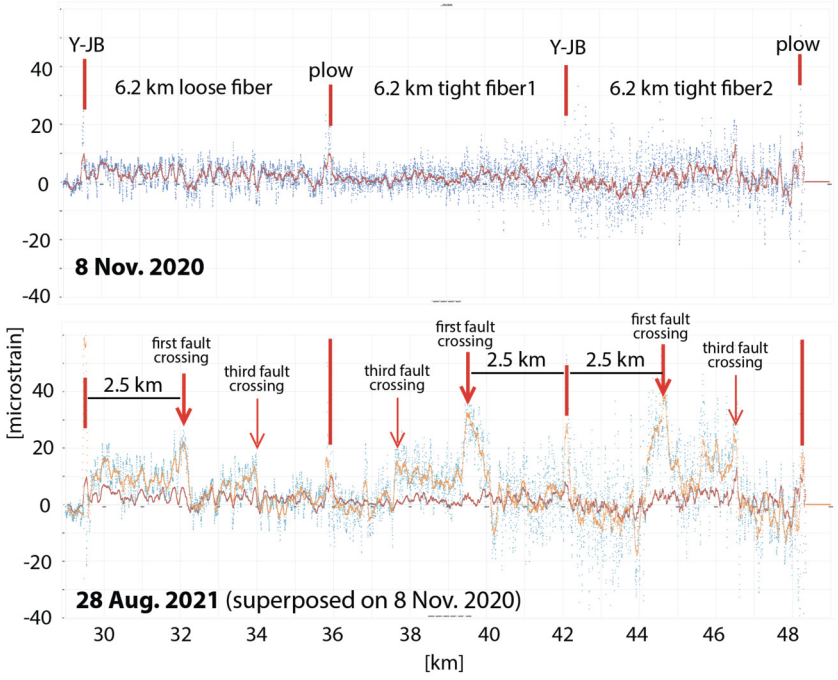

Fig. 3. BOTDR (relative strain measurements) along the three-fold loop of the 6.2-km long strain cable, with respect to the 28 Oct. 2020 baseline. Small colored dots are individual values every 2 m, the colored curves are a 100 m sliding average. Thin vertical lines are km in distance along the cable with respect to the INFN-LNS port laboratory (0 km). (top) The measurement from 8 Nov. 2020 (light blue dots and red curve) shows no systematic deviation from the 0 microstrain horizontal axis. (bottom) The measurement from 28 Aug. 2021 (green dots and purple sliding average curve) is superposed on the 8 Nov. 2020 data (red curve), and shows marked peaks at the first fault crossing (2500 m from the Y-JB) and at the third fault crossing (4300 m from the Y-JB). The signals in the tight fibers are +30 to +40 microstrain at the first fault crossing and +15 to +25 microstrain at the third fault crossing. The corresponding signals for the loose fiber are about half the amplitude, +20 and +10 to +15 microstrain, respectively, at the first and third fault crossings.

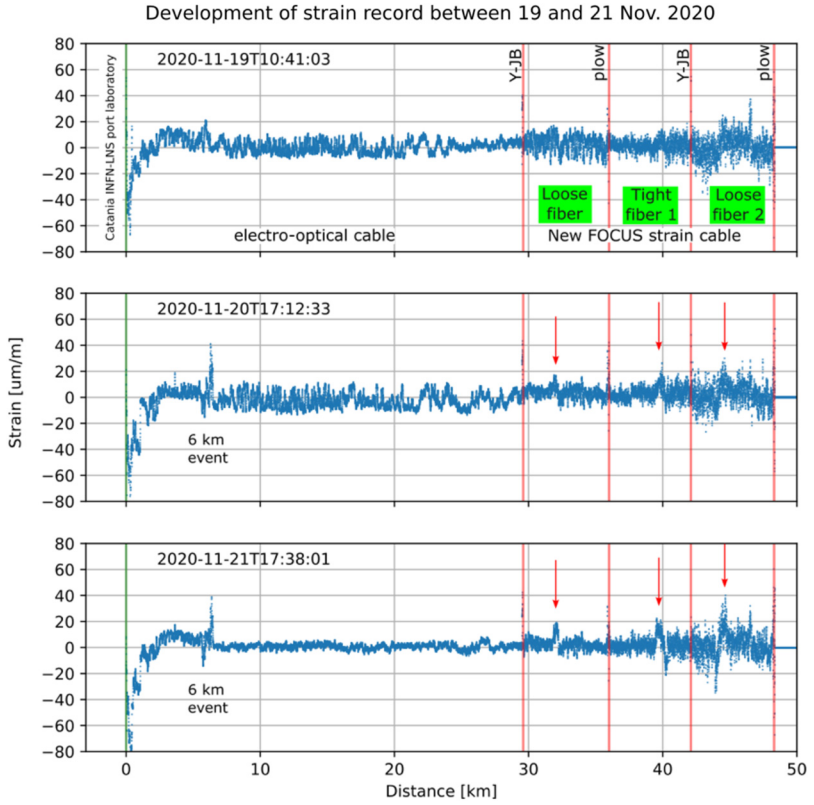

Fig. 4. BOTDR observations along the entire optical path of 48 km, representing the 29-km long electro-optical cable and the triple loop (3 × 6.2 km) within the FOCUS fiber optic strain cable for the 19th, 20th and 21st of Nov. 2020 (with respect to the 28 Oct. 2020 baseline). The green line at 0 km represents the INFN-LNS port laboratory. The red vertical lines indicate the positions of the Y-junction box (Y-JB) and the deep-sea plow. Note how elongation peaks develop at the first fault crossing (marked by the red arrows). A dual signal (contraction and elongation) event is detected at 6 km distance from Catania on 20 and 21 Nov. 2020 on the electro-optical cable.

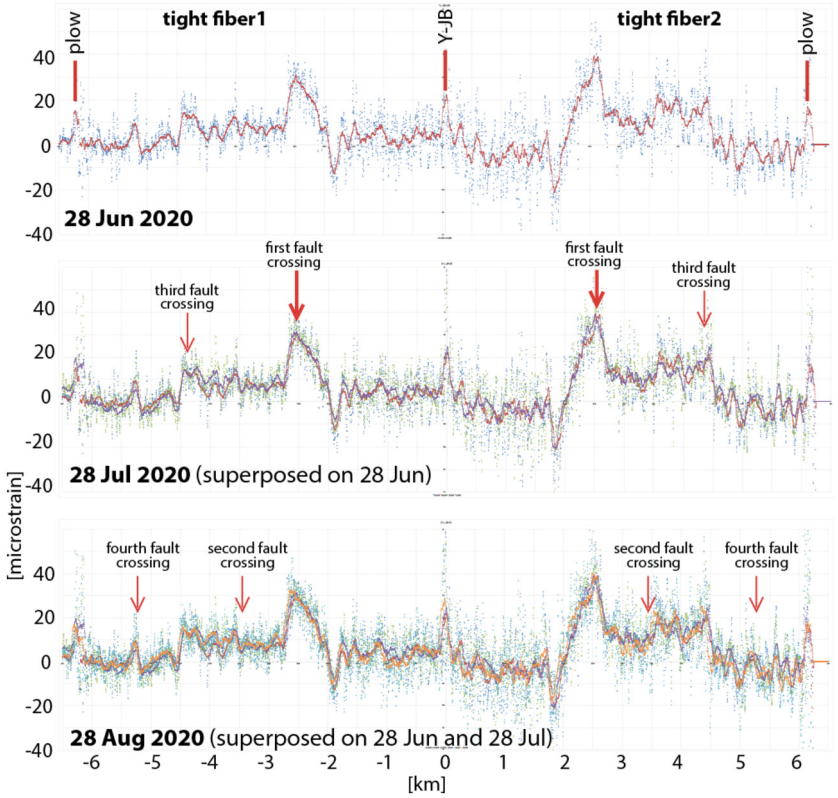

Fig. 5. BOTDR observations along the two tightly bound fibers from 28 June, 28 July and 28 August 2021 (with respect to the 28 Oct. 2020 baseline). 0 km represents the position of the Y-junction box (Y-JB). This shows the repeatability of the measurements when no significant perturbation occurs. Red arrows indicate the locations of the fault crossings, with elongation peaks present at the first and third fault crossings (2.5 km and 4.3 km cable distance). No distinct signals (neither elongation peaks nor shortening minima) are observed at the second and fourth fault crossings (3.45 km and 5.2 km cable distance).

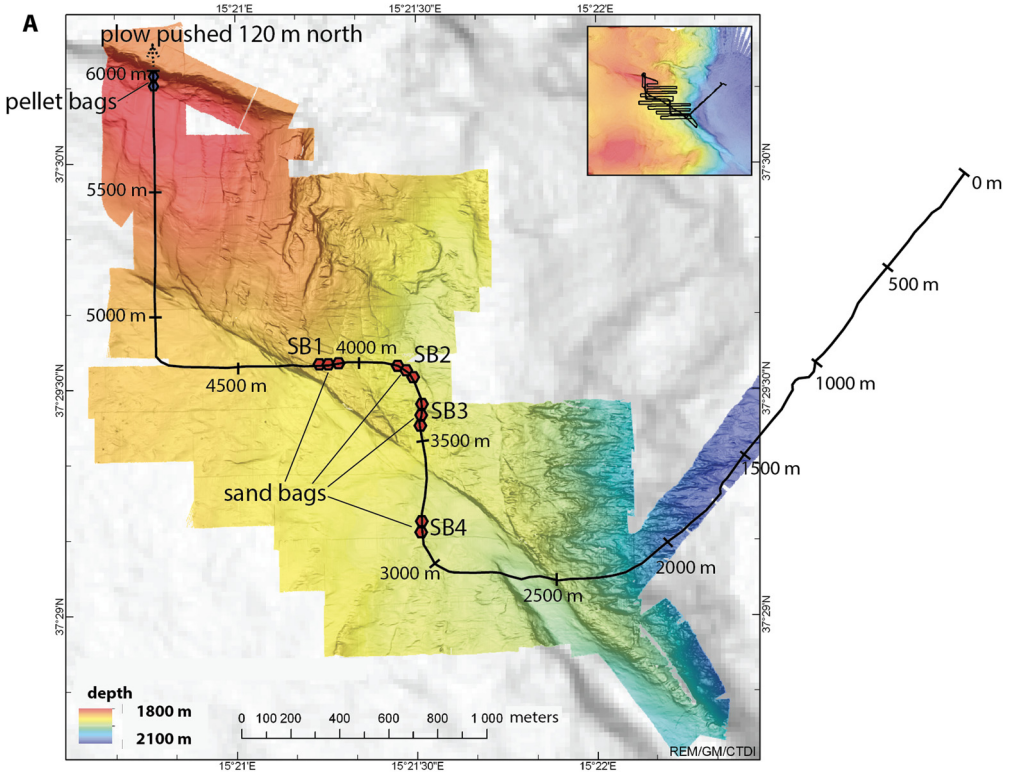

Fig. 6. Sandbag experiment begun on 2 Sept. 2021. A: Location map of the cable track (black) on the microbathymetric map. The four sand-bag drop segments are labeled SB1 to SB4 and pellet bags were placed on a segment near the NW termination (at 5.9 km cable distance). Only the distal portion of the strain cable (from 3.2 km to 6 km) was affected by this experiment. B: Picture of seafloor operations with the Fugro ROV, placing 25-kg sand-bags on top of the FOCUS fiber optic strain cable.

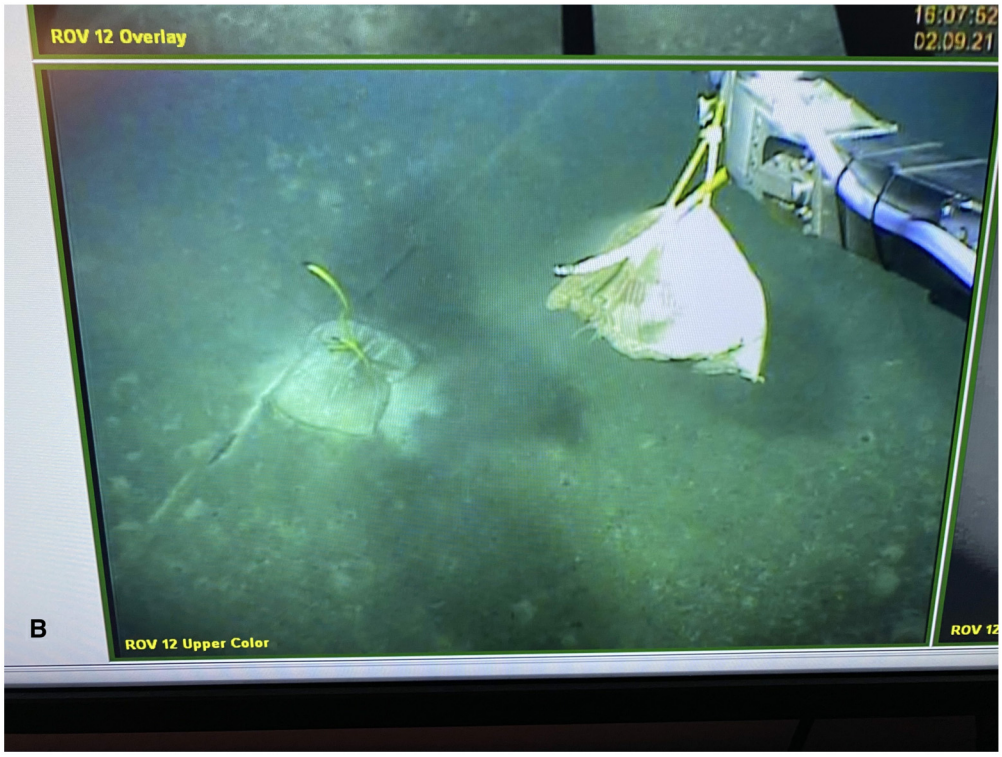

Fig. 6. (*continued*)

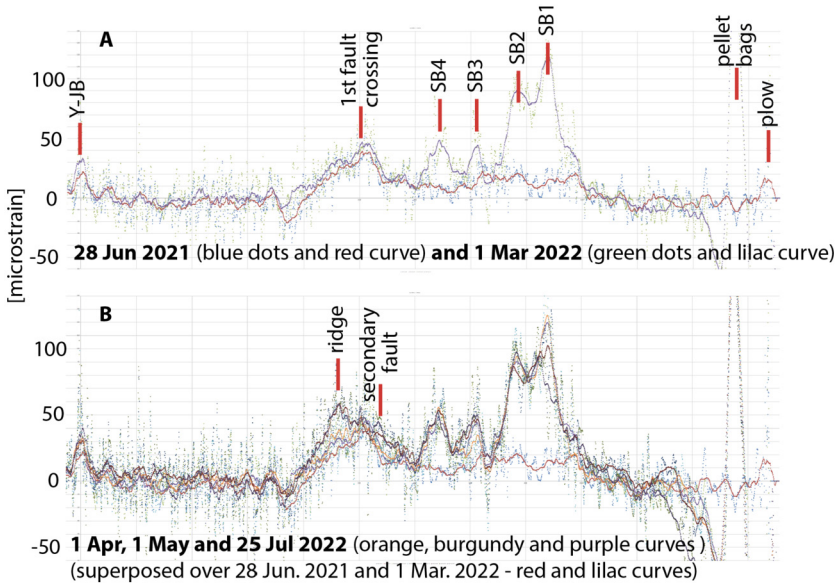

Fig. 7. BOTDR (relative strain measurements) for the second tight fiber with respect to the 28 Oct. 2020 baseline. A) Observations for 28 Jun. 2021 and 1 Mar. 2022. Blue dots and green dots are individual values every 2 m, the red curve and lilac curve are 100 m sliding averages. Thin vertical lines are 500 m in distance along the cable with respect to the Y-junction box (0 km). The positions of the sand-bag (SB1–SB4) and pellet bag drop areas along the cable are shown. B) BOTDR Observations for 1 Apr. (orange curve) 1 May (burgundy curve) and 28 Jul. (purple curve) superposed over the 28 Jun. 2021 and 1 Mar. 2022 data. Small dots are individual values every 2 m, colored curves are 100 m sliding averages.

with a peak amplitude of +50 to +55 micro-strain. Taken over the 21-month period (Oct. 2020–July 2022) the total signal represents an elongation of 2.5 cm. The signal has evolved and widened and in July 2022 is centered on the morphological ridge about 200 m to the east of the first fault crossing and extends to a secondary fault splay to the west (Fig. 7B) forming the SW boundary of a morphological trough, and see also maps (Figs. 2, 6A).

BOTDR observations for the distal 3 km (from 3.2 km to 6.2 km cable distance) show the effect of the bag drops in the 5 areas. For the four sand-bag sections, strain signals of +50 to +120 micro-strain are observed in the year following the bag drops (see signals from 1 March, 1 April, 1 May and 25 July 2022 in Figs. 7 A, B). The strain perturbation in the pellet bag section is even greater, reaching values of +250 microstrain. In all areas the signal is strongly positive, indicating the cable has been elongated by being weighed down and pushed vertically downwards into the soft sediments. The total elongation per 120 m segment ranges from about 1 cm to 4 cm, but the area of effect is about 250 m wide (twice as

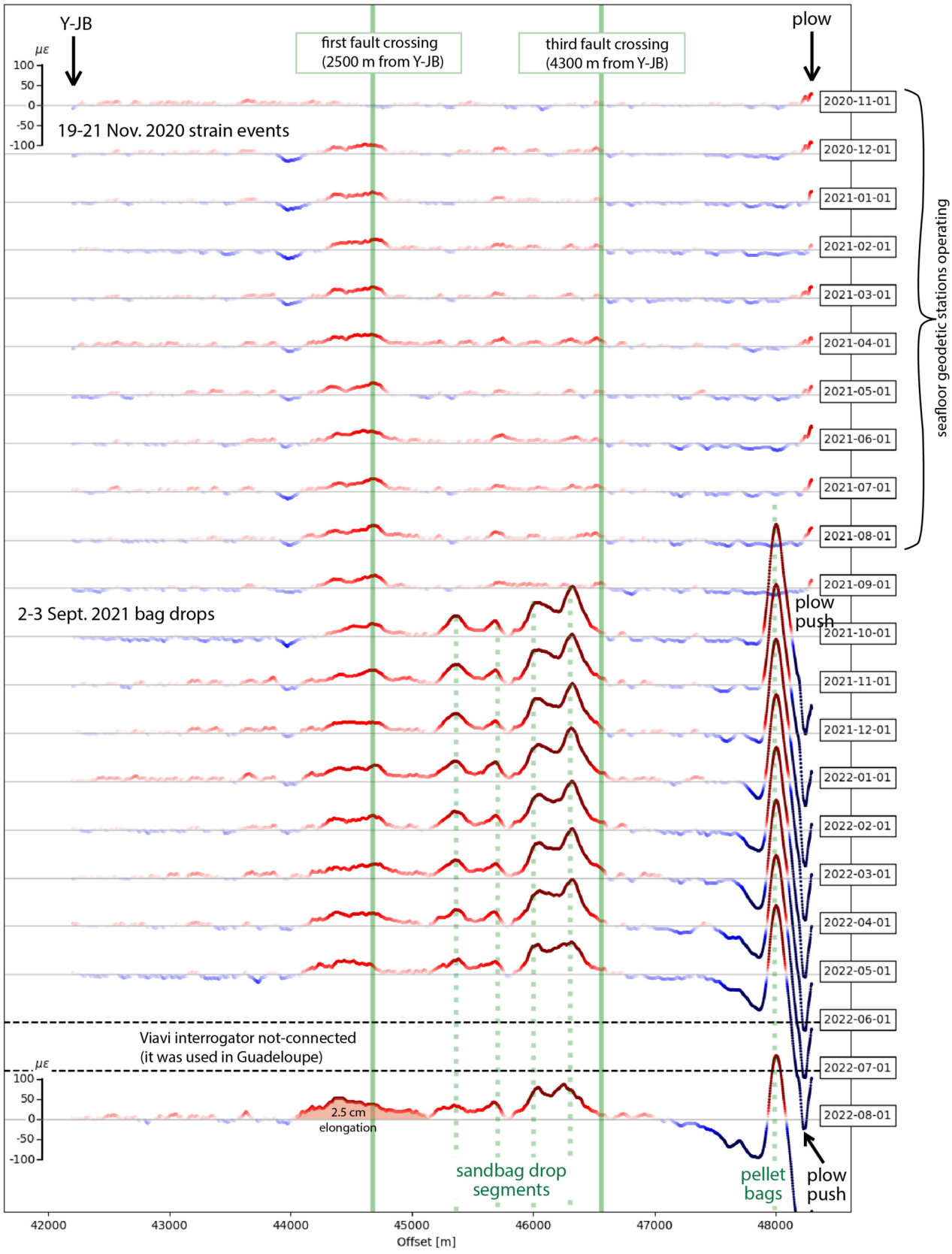

Fig. 8. BOTDR (relative strain measurements) for the second tight fiber with respect to the 28 Oct. 2020 baseline represented over 21 months (from 1 Nov. 2020 to 1 Aug. 2022). The positions of the first and third fault crossings are indicated by the light green vertical lines. The sand bag and pellet bag drop segments are indicated by vertical dotted magenta lines and the plow push is indicated by the vertical dashed orange line. The amplitude of most of the deformation signals at the bag drop locations diminishes over time, as the elastic properties of the cable allow the fibers to readjust. For instance the signal at the fourth sand bag segment initially 150 microstrain, drops to 100 microstrain after 10 months and at the pellet bags it drops from 300 microstrain to 200 microstrain. Note also the 30–40 microstrain signal at the first fault crossing which appears already on 1 Dec. 2020, increases in amplitude to 50 microstrain and broadens in time.

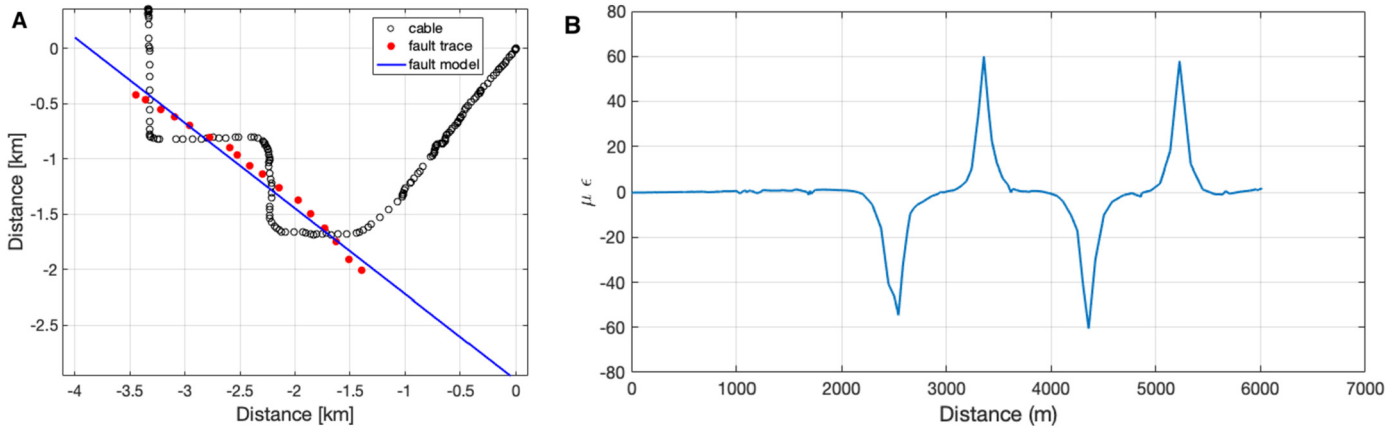

Fig. 9. Elastic dislocation modeling for a vertically dipping dextral strike-slip fault oriented NW-SE and extending from 50 m depth below the seafloor to 5.05 km sub-seafloor depth. A: actual fault trace (red dots) and modeled fault trace (blue line) and cable track geometry (small black circles), B: Predicted strain signal for 4 cm of dextral fault slip. Note the positive (elongation) strain signals at the first and third fault crossings, and the negative (axial shortening) strain signals at the second and fourth fault crossings.

long as the section where the bags were placed). The BOTDR strain observations plotted once per month over the 21-month observation period show the strain evolution through time (Fig. 8). In the 5–10 months following the bag drop experiment, significant readjustment occurs, and most of the elongation peaks diminish, for instance from +150 microstrain to +100 microstrain (in sand-bag drop segment SB1) while the +250 microstrain peak in the pellet bag drop segment drops to +180 microstrain after 10 months. (Fig. 8).

4. Discussion

4.1. Elastic dislocation modeling

We used an elastic dislocation model to simulate how the tectonic movement on the Alfeo fault would produce strain on the cable, for the deployed cable geometry. The fault is represented by two triangles making a vertical rectangular fault starting at a depth of 50 m, with a width and length of 5 km and a dextral (right-lateral) slip of 4 cm. The location of the fault (blue line Fig. 9A) is based on the geo-referenced fault trace picked from the high-resolution bathymetric data (red dots Fig. 9A). The media is assumed to respond purely elastically to the dislocation and have a Poisson ratio of 0.25. Assuming the cable is perfectly coupled with the seafloor the strain tensor is calculated using the elastic dislocation code of Nikkhoo and Walter (2015). The strain tensor is then projected such that the x-axis is parallel to the cable orientation whereby ε_{xx} is equal to the longitudinal strain of the cable (Martin, 2018; Currenti et al., 2021). Changing the amount of slip will increase/decrease the amplitude of strain, changing the depth of the slipping surface will alter the shape of the strain pattern – i.e. the peaks become larger and narrower the closer to the surface the dislocation is. As can be seen, the fault slip model predicts elongation at the first and third fault crossings and axial shortening at the second and fourth fault crossings (Fig. 9B).

4.2. Possible sources of deformation at the seafloor

Over the first 10 months, two marked elongation peaks (respectively +40 and +25 microstrain) were observed at the first and third fault crossings. A minimum (−20 micro-strain) is observed at 1800 m cable distance from the Y-junction box, along a steep slope marked by E-W oriented gullies in an area of rugged seafloor relief. The expected types and positions of strain signals are illustrated schematically in Fig. 10.

As discussed above, for a dextral strike-slip fault movement, elongation should be observed at the first and third fault crossings (Fig. 10, upper panel). This is the pattern we observe (Figs. 3, 4, 5). Conversely, shortening should hypothetically be observed at the second and fourth fault crossings. We do not observe distinct axial shortening signals at the second and fourth fault crossings (Fig. 5). However, in order to observe negative strain (axial shortening) along a straight section of cable, the cable must be well buried, with a homogeneous, constant tension, and then an appropriate fault movement will cause the tension to drop and the cable to shorten. Given the difficulties encountered during cable deployment and the large portions (>50%) of the cable path where the cable is unburied, resting on the seafloor or spanning between rugged relief (Suppl. Fig. 2B), this condition is seldom fulfilled. Therefore, we probably cannot observe negative strain along large portions of the cable.

Another possible source of deformation for the submarine cable is downslope current along the morphological channel at the base of fault scarp (Fig. 10, central panel). If such a current follows the fault scarp along its entire length, it would cause elongation signals centered over the channel at all locations where the cable is unburied and exposed to seabottom currents. This is not exactly the pattern observed in the first 10 months of BOTDR recordings (Fig. 3, Fig. 5). The peak at 2500 m cable distance is centered on the fault, and not over the channel. The peak around 4200–4500 m cable distance does extend somewhat past the fault (located at 4300 m) and into the channel. No clear elongation signal is observed at the second and fourth fault crossings, at cable distances of 3450 m and 5200 m, respectively (Fig. 5, bottom panel red arrows) (see also suppl. Fig. 4).

Finally, shortening might be expected to occur due to post-deployment readjustment of the cable, as it slips off rugged relief and this should occur primarily in the more strongly curved portions of the cable (Fig. 10, bottom panel). The shortening observed at 1800 m in the steep gullies (Figs. 3, 5) appears to be consistent with this type of strain mechanism. This negative strain signal (axial shortening) dissipates gradually over the next 9–12 months (Fig. 8).

It is also worth noting that thermal variations can potentially influence BOTDR measurements, and this is indeed observed in the portion of the electro-optical cable closest to the INFN-LNS port laboratory in Catania (a brief onland portion and a 1–2 km long shallow water portion). However, in the deep offshore domain (1800–2100 m) where the FOCUS fiber-optic strain cable is deployed, the annual seabottom temperature is very stable, typically fluctuating from 13.78–13.88 °C (based on 9–23 months of temperature recordings from our seafloor geodetic stations. This

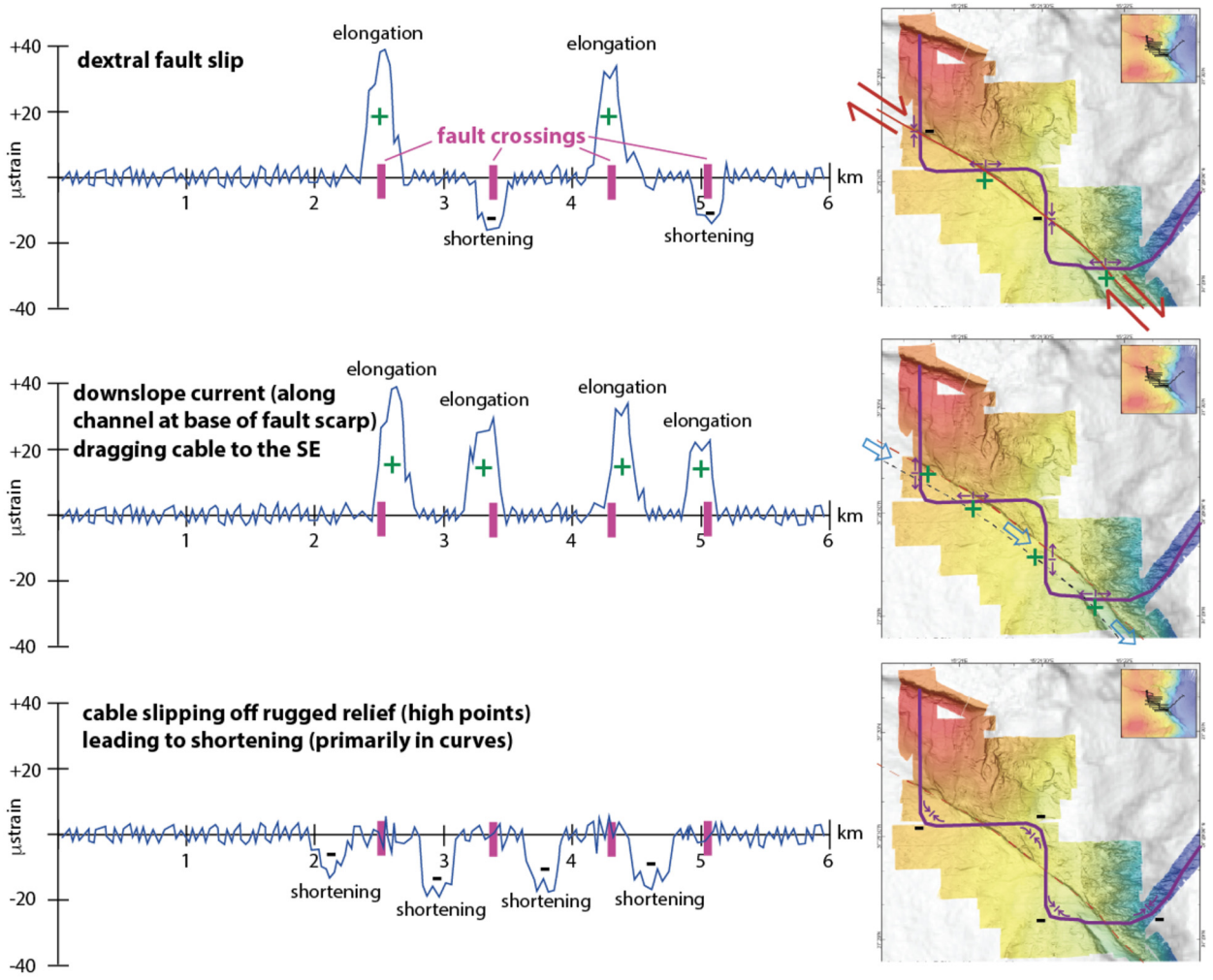

Fig. 10. Examples of deformation mechanisms which could affect the cable and idealized (hypothetical) strain signals which could result. The short wavelength, small amplitude (<5 microstrain) fluctuations represent the noise. Top panel: dextral strike-slip fault movement causing alternating elongation and shortening signals centered at the fault intersections. Note that in order to observe negative strain (axial shortening), a homogeneous, constant tension is required in the cable after deployment/burial.; Central Panel: downslope current along the morphological channel at base of fault scarp causing elongation signals centered over the channel; Bottom Panel: post-deployment readjustment of the cable, slipping off rugged relief and causing shortening primarily in the strongly curved portions of the cable.

represents less than 2 microstrain. Furthermore, a thermal perturbation recorded by the cable should be transient, not permanent.

4.3. Seafloor geodesy (distance-ranging)

Available distance ranging data from a network of 8 acoustic transponders (Canopus model CRT142, manufactured by iXblue/exail) on the seafloor (Fig. 2), while spanning only the period Oct. 2020–Aug. 2021 (Fig. 8), do not show any statistically significant change in baseline lengths during Nov. 2020 (Royer et al., 2022) when the first BOTDR elongation event occured. A second network of 5 Sonardyne acoustic transponders operated by Geomar is located halfway between the FOCUS fiber-optic cable and the coast of Mount Etna, some 15 km to the NW in water depths of 1000–1200 m (see Urlaub et al., 2018). This network did not show any abrupt relative displacements in November 2020 either (Urlaub pers. comm.).

4.4. Seabottom currents and seismicity

The dual shortening – elongation event described in section 3.1 (Fig. 4), affecting the MEOC 6 km from the port of Catania, occurred at the shelf edge in 200–300 m water depth (small white star, Fig. 1), at a distance of 3–5 km from the nearest Mount Etna flank faults. Somehow it seems temporally related to the elongation events observed on the FOCUS strain cable. One plausible scenario is that there was a submarine landslide here at the shelf-break and that a turbidity current ensued, which transited along the trough at the base of the fault scarp, causing elongation at the first and third fault crossings. The disturbance did not affect the cable at the second and fourth fault crossings, possibly because the cable was better buried beneath the sediments here, protecting it from seabottom currents. Another scenario is that slow fault-slip occurred along different portions of the Mount Etna flank faults and along the North Alfeo fault, and that this movement destabilized the sediments at the shelf break, causing a small landslide here (small white star on Fig. 1), which affected the electro-optical cable.

We examined the local seismicity during the period 19–21 Nov. 2020 (Suppl. Table 1) to determine if it could have played a role in strain variations along the cable. A small, shallow earthquake (magnitude 2.6 and 8 km depth) occurred on 21 Nov. 2020 (13:55 UTC) in Santa Venerina village about 10 km north of the cable, along the coast on the SE flank of Mount Etna (Fig. 1 green star, see also Suppl. Fig. 7). This event is just prior to the 21 Nov. 2020 BOTDR data shown (Fig. 4 bottom), but occurred about 1 day after the disturbance on the MEOC, already visible on the 20 Nov. 2020 record from 17:12 (Fig. 4 middle, and Suppl. Figs. 4 and 5).

Thus, the earthquake itself could not have triggered the submarine landslide. Further observations (for instance in-situ observations of the cable at the seafloor, or analysis of local land-based geodetic data) are necessary to distinguish between the two competing hypotheses. Ongoing work (begun in Feb. 2023) will also provide measurement of the in-situ currents at the seafloor near the first cable crossing using an Acoustic Doppler Current Profiler (ADCP) current meter. Regional seismicity and micro-seismicity are currently under investigation with a combined onshore (INGV permanent network + 13 temporary land-stations) and offshore (29 ocean-bottom seismometers) network deployed from Jan. 2022 to Feb. 2023. The results of this seismological study (in progress) are expected to improve earthquake hypocenter locations and highlight seismically active structures. Currently available hypocenter maps based solely on locations from land-stations have relatively high uncertainties in location and depth (±10–20 km) resulting in a broad diffuse distribution of seismicity offshore (Suppl. Fig. 8).

5. Conclusions

A dedicated fiber-optic strain cable was deployed 25 km offshore Catania Sicily at 2100 m water depth, connected to the Test Site South (TSS) termination of the Main Electro Optical Cable operated by INFN-LNS. The strain cable, interrogated by a VIAVI Brillouin Optical Time Domain Reflectometer, detected two episodes of deformation on the seafloor. The first episode, representing about 1–1.5 cm of elongation occurred from 19–21 Nov. 2020, with a signal of +40 microstrain amplitude (expressed over a 400–500 m long section of cable), centered on the first crossing of the North Alfeo fault (2500 m cable distance from the Y-JB). A secondary peak, with an amplitude of +25 microstrain was observed at the third fault crossing (4300 m from the Y-JB). The elongation peak is more readily observed in the tight fibers, but can also be observed in the loose fiber, with an amplitude of about +20 microstrain (half the signal compared to the tight fibers). This result implies that existing submarine telecom cables (which use exclusively loosely bound fibers) are very likely suitable for deformation monitoring. During the period Sept. 2021 to late July 2022, a larger, broader deformation signal developed across a nearly 1-km long section of cable (from 2.0–3.0 km cable distance from the Y-JB), with a peak amplitude of +50 to +55 microstrain. Taken over the 21 months, the total signal represents an elongation of 2.5 cm (Fig. 8). This broader signal is centered 200 m east of first fault crossing, on a morphological ridge and encompasses the trough below the fault scarp and a secondary fault splay to the west. These strain signals are consistent with dextral strike-slip motion along the North Alfeo Fault, expressed more strongly at the first fault crossing. However, a seabottom current (dense shelf water cascade or submarine landslide/turbidity current) affecting the unburied portions of the cable may have caused the cable elongation. Available distance ranging data from a network of acoustic transponders on the seafloor, while spanning only the first 9 months of the laser reflectometry observation period, show no significant dextral strike-slip movement in Nov. 2020 (Royer et al., 2022). During the period Sept. 2021 to Aug. 2022, the distal portion of the strain cable (3.2 km–6.0 km cable distance) was the site of a sandbag experiment, whose primary purpose was to increase the coupling between the cable and the soft unconsolidated sediments making the BOTDR more sensitive to deformation. The results of the experiment, with strain signals of +50 to +120 micro-strain, indicate elongations ranging from 1 cm to 4 cm per test segment. These elongations were commonly followed by cable and fiber relaxation (causing axial shortening) over the next 10 months, locally erasing 10–30% of the initial signal. The sandbag experiment demonstrates the sensitivity of the strain cable to manmade perturbations while suggesting it is important to perform repeat measurements every few months before cable readjustment erases part of the signal. These preliminary results are encouraging with respect to the application of BOTDR observations for monitoring movements on the seafloor and for detecting natural or manmade perturbations of submarine cables. Finally, the successful observation of strain, despite a largely unburied cable, with multiple spans and poor coupling to the seafloor, implies that submarine telecom cables, which are unburied in water depths exceeding 500 m, could potentially be used for strain monitoring.

CRediT authorship contribution statement

MAG – obtained project funding and shiptime, and drafted the manuscript. LQ and SA performed the laser interferometry measurements, ensured a remotely operated link to the interrogator with continuous near real-time data acquisition and storage. SM and FK contributed to shipboard operations during the cable deployment cruise FocusX1. GR provided onshore logistical support during cable connection during the FocusX1 cruise and is the scientific liaison to the seafloor cabled observatory operated by INFN-LNS. JYR is responsible for the network of 8 seafloor geodetic stations and drafted supplementary Figure 3. GB is the tectonics expert (for active faults) and national partner who aided in mission logistics and obtaining authorization to work in Italian waters. SK and FG provided seismic data and bathymetric data for selecting the cable track to cross a clearly defined segment of the submarine North Alfeo fault. HK and MU provided published and unpublished data from the nearby network of seafloor geodetic stations deployed and operated by Geomar. GC extracted, filtered and plotted BOTDR data, drafting several figures. All co-authors read and revised the manuscript.

Declaration of competing interest

The authors declare that they have no known competing financial interests or personal relationships that could have appeared to influence the work reported in this paper.

Data availability

Data will be made available on request.

Acknowledgements

We thank the captain Philippe Moimeaux, the ROV team and the crew of the R/V PourquoiPas?, whose excellent work during the FocusX1 expedition was crucial to deploying the cable, despite multiple difficulties encountered. Thanks also to the captain and crew of the Fugro vessel the Handin Tide for their professional work. This work is funded by the European Research Council Advanced Grant FOCUS #786304. MU has received funding from the European Research Council (ERC) under the European Union's Horizon 2020 research and innovation programme (Starting Grant, #948797).

Appendix A. Supplementary material

Supplementary material related to this article can be found online at https://doi.org/10.1016/j.epsl.2023.118230.

References

Argnani, A., Bonazzi, C., 2005. Malta escarpment fault zone offshore eastern Sicily: Pliocene-quaternary tectonic evolution based on new multichannel seismic data: Offshore eastern Sicily. Tectonics 24, TC4009. https://doi.org/10.1029/2004TC001656.

Bonforte, A., Guglielmino, F., Colteli, M., Ferretti, A., Puglisi, G., 2011. Structural assessment of Mount Etna volcano from Permanent Scatterers analysis. Geochem. Geophys. Geosyst. 12, Q02002. https://doi.org/10.1029/2010GC003213.

Cernobori, L., Hirn, A., McBride, J.H., Nicolich, R., Petronio, L., Romanelli, M., STREAMERS/PROFILES Working Groups, 1996. Crustal image of the Ionian basin and its Calabrian margins. Tectonophysics 264, 175–189.

Currenti, G., Jousset, P., Napoli, R., Krawczyk, C., Weber, M., 2021. On the comparison of strain measurements from fibre optics with a dense seismometer array at Etna volcano (Italy). Solid Earth 12, 993–1003. https://doi.org/10.5194/se-12-993-2021.

Dellong, D., Klingelhoefer, F., Kopp, H., Graindorge, D., Margheriti, L., Moretti, M., Murphy, S., Gutscher, M.-A., 2018. Crustal structure of the Ionian Basin and eastern Sicily margin: results from a wide-angle seismic survey. J. Geophys. Res., Solid Earth 123, 2090–2114. https://doi.org/10.1002/2017JB015312.

Faccenna, C., Piromallo, C., Crespo-Blanc, A., Jolivet, L., Rossetti, F., 2004. Lateral slab deformation and the origin of the western Mediterranean arcs. Tectonics 23, TC1012. https://doi.org/10.1029/2002TC001488.

Favali, P., Chierici, F., Marinaro, G., Giovanetti, G., Azzarone, A., Beranzoli, L., De Santis, A., Embriaco, D., Monna, S., Lo Bue, N., et al., 2013. NEMO-SN1 abyssal cabled observatory in the western Ionian Sea. IEEE J. Ocean. Eng. 38 (2), 358–374. https://doi.org/10.1109/joe.2012.222.4536.

Goes, S., Giardini, D., Jenny, S., Hollenstein, C., Kahle, H.G., Geiger, A., 2004. A recent tectonic reorganization in the south-central Mediterranean. Earth Planet. Sci. Lett. 226, 335–345. https://doi.org/10.1016/j.epsl.2004.07.038.

Govers, R., Wortel, M.J.R., 2005. Lithosphere tearing at STEP faults: response to edges of subduction zones. Earth Planet. Sci. Lett. 236, 505–523.

Gutscher, M.-A., Dominguez, S., Mercier de Lepinay, B., Pinheiro, L., Gallais, F., Babonneau, N., Cattaneo, A., LeFaou, Y., Barreca, G., Micallef, A., Rovere, M., 2016. Tectonic expression of an active slab tear from high-resolution seismic and bathymetric data offshore Sicily (Ionian Sea). Tectonics 35 (1). https://doi.org/10.1002/2015TC003898.

Gutscher, M.-A., Kopp, H., Krastel, S., Bohrmann, G., Garlan, T., Zaragosi, S., Klaucke, I., Wintersteller, P., Loubrieu, B., LeFaou, Y., San Pedro, L., Dominguez, S., Rovere, M., Mercier de Lepinay, B., Ranero, C., Sallares, V., 2017. Active tectonics of the Calabrian subduction revealed by new multi-beam bathymetric data and high-resolution seismic profiles in the Ionian Sea (central Mediterranean). Earth Planet. Sci. Lett. 461, 61–72. https://doi.org/10.1016/j.epsl.2016.12.020.

Gutscher, M.-A., Royer, J.-Y., Graindorge, D., Murphy, S., Klingelhoefer, F., Aiken, C., Cattaneo, A., Barreca, G., Quetel, L., Riccobene, G., Petersen, F., Urlaub, M., Krastel, S., Gross, F., Kopp, H., Moretti, M., Berenzoli, L., 2019. Fiber optic monitoring of active faults at the seafloor: the FOCUS project, photoniques. EDP Sci., 32–37. https://doi.org/10.1051/photon/2019S432.

Gvirtzman, Z., Nur, A., 1999. The formation of Mount Etna as the consequence of slab rollback. Nature 401, 782–785.

Jiang, X., Gao, Y., Wu, Y., Lei, M., 2016. Use of Brillouin optical time domain reflectometry to monitor soil-cave and sink hole formation. Environ. Earth Sci. 75, 225. https://doi.org/10.1007/s12665-015-5084-1.

Jousset, P., Reinsch, T., Ryberg, T., Blanck, H., Clarke, A., Aghayef, R., Hersir, G.P., Henninges, J., Weber, M., Krawcyk, C.M., 2018. Dynamic strain determination using fibre-optic cables allows imaging of seismological and structural features. Nat. Commun. 9, 2509. https://doi.org/10.1038/s41467-018-04860-y.

Lindsey, N.J., Martin, E.R., Dreger, D.S., Freifeld, B., Cole, S., James, S.R., Biondi, B.L., Ajo-Franklin, J.B., 2017. Fiber-optic network observations of earthquake wavefields. Geophys. Res. Lett. 44. https://doi.org/10.1002/2017GL075722.

Lindsey, N.J., Dawe, T.C., Ajo-Franklin, J.B., 2019. Illuminating seafloor faults and ocean dynamics with dark fiber distributed acoustic sensing. Science 366, 1103–1107. https://doi.org/10.1126/science.aay5881.

Maesano, F.E., Tiberti, M.M., Basili, R., 2020. Deformation and fault propagation at the lateral termination of a subduction zone: the Alfeo Fault System in the Calabrian arc, southern Italy. Front. Earth Sci. 8, 107. https://doi.org/10.3389/feart.2020.00107.

Maraval, D., Gabet, R., Jaouen, Y., Lamour, V., 2017. Dynamic optical fiber sensing with Brillouin optical time domain reflectometry: application to pipeline vibration monitoring. J. Lightwave Technol. https://doi.org/10.1109/JLT.2016.2614835.

Marra, G., Clivatti, C., Luckett, R., Tampellini, A., Kronjäger, J., Wright, L., Mura, A., Levi, F., Robinson, S., Xuereb, A., Baptie, B., Calonico, D., 2018. Ultrastable laser interferometry for earthquake detection with terrestrial and submarine cables. Science 361. https://doi.org/10.1126/science.aat4458.

Marra, G., Fairweather, D.M., Kamalov, V., Gaynor, P., Cantono, M., Mulholland, S., Baptie, P., Baptie, B., Castellanos, J.C., Vagenas, G., Gaudron, J.-O., Kronjäger, J., Hill, I.R., Schioppo, M., Barbeito Edreira, I., Burrows, K.A., Clivati, C., Calonico, D., Curtis, A., 2022. Optical interferometry-based array of seafloor environmental sensors using a trans-oceanic submarine cable. Science 376. https://doi.org/10.1126/science.abo1939.

Martin, E., 2018. Passive imaging and characterization of the subsurface with distributed acoustic sensing. PhD thesis. Stanford University, Stanford, CA, USA.

Muanenda, Y., Oton, C.J., Di Pasquale, F., 2019. Application of Raman and Brillouin scattering phenomena in distributed optical fiber sensing. Front. Phys. 7, 155. https://doi.org/10.3389/fphy.2019.00155.

Nikkhoo, M., Walter, T.R., 2015. Triangular dislocation: an analytical, artefact-free solution. Geophys. J. Int. 201 (2), 1119–1141.

Polonia, A., Torelli, L., Mussoni, P., Gasperini, L., Artoni, A., Klaeschen, D., 2011. The Calabrian arc subduction complex in the Ionian Sea: Regional architecture, active deformation and seismic hazard. Tectonics 30, TC5018. https://doi.org/10.1029/2010TC002821.

Riccobene, G., 2009. Long-term measurements of acoustic background noise in very deep sea. Nucl. Instrum. Methods Phys. Res. A 604, S149–S157.

Royer, J.-Y., et al., 2022. Active strike-slip fault monitoring using marine geodesy, Offshore Mt Etna, Sicily (Italy). In: Proc. EGU General Assembly, vol. 2022, pp. EGU22–EGU8264.

Sun, Y., Shi, B., Zhang, B., Tong, H., Wei, G., Xu, H., 2016. Internal deformation monitoring of slope based on BOTDR. J. Sens., 9496285. https://doi.org/10.1155/2016/9496285.

Sladen, A., Rivet, D., Ampuero, J.P., De Barros, L., Hello, Y., Calbris, G., Lamare, P., 2019. Distributed sensing of earthquakes and ocean-solid Earth interactions on seafloor telecom cables. Nat. Commun. 10, 5777. https://doi.org/10.1038/s41467-019-13793-z.

Urlaub, M., Petersen, F., Gross, F., Bonforte, A., Puglisi, G., Guglielmino, F., Krastel, S., Lange, D., Kopp, H., 2018. Gravitational collapse of mount Etna's south-eastern flank. Sci. Adv. 4, eeat9700. https://doi.org/10.1126/sciadv.aat9700.

Wang, H.F., Zeng, X., Miller, D.E., Fratta, D., Feigl, K.L., Thurber, C.H., Mellors, R.J., 2018. Ground motion response to an ml 4.3 earthquake using co- located distributed acoustic sensing and seismometer arrays. Geophys. J. Int. 213, 2020–2036.

Williams, E.F., et al., 2019. Distributed sensing of microseisms and teleseisms with submarine dark fibers. Nat. Commun. 10, 5778. https://doi.org/10.1038/s41467-019-13262-7.

Yu, C., Zhan, Z., Lindsey, N.J., Ajo-Franklin, J.B., Robertson, M., 2019. The potential of DAS in teleseismic studies: insights from the Goldstone experiment. Geophys. Res. Lett. 46, 1320–1328.

Zhao, L., Li, Y., Xu, Z., Yang, Z., Lü, A., 2014. On-line monitoring system of 110 kV submarine cable based on BOTDR. Sens. Actuators A 216, 28–35. https://doi.org/10.1016/j.sna.2014.04.045.

Zumberge, M.A., Hatfield, W., Wyatt, F.K., 2018. Measuring seafloor strain with an optical fiber interferometer. Earth Space Sci. 5, 71–379. https://doi.org/10.1029/2018EA000418.